Nanotechnology

PAPER

# Manifestation of plasmonic response in the detection of sub-terahertz radiation by graphene-based devices

IOP Publishing

Nanotechnology

Nanotechnology **29** (2018) 245204 (8pp)

https://doi.org/10.1088/1361-6528/aab7a5

# Manifestation of plasmonic response in the detection of sub-terahertz radiation by graphene-based devices

**I A Gayduchenko[1,2,12], G E Fedorov[1,3,12], M V Moskotin[1], D I Yagodkin[3], S V Seliverstov[1], G N Goltsman[1,5], A Yu Kuntsevich[4,5], M G Rybin[6], E D Obraztsova[6], V G Leiman[7], M S Shur[8], T Otsuji[9] and V I Ryzhii[9,10,11]**

[1] Physics Department, Moscow State University of Education, Moscow 119991, Russia
[2] National Research Center 'Kurchatov Institute', 123182, Moscow, Russia
[3] Department of General Physics, Moscow Institute of Physics and Technology, Dolgoprudny 141700, Russia
[4] P.N. Lebedev Physical Institute, 38 Vavilov str., Moscow, 119991, Russia
[5] National Research University Higher School of Economics, 101000, Moscow, Russia
[6] Prokhorov General Physics Institute, 38 Vavilov str., Moscow, 119991, Russia
[7] Laboratories of 2D Materials' Optoelectronics and Nanooptics and Plasmonics, Moscow Institute of Physics and Technology, Dolgoprudny 141700, Russia
[8] Departments of Electrical, Computer, and System Engineering and Physics, Applied Physics, and Astronomy, Rensselaer Polytechnic Institute, Troy, NY 121180, United States of America
[9] Research Institute of Electrical Communication, Tohoku University, Sendai 980-8577, Japan
[10] Institute of Ultra High Frequency Semiconductor Electronics of RAS, Moscow 117105, Russia
[11] Center for Photonics and Infrared Engineering, Bauman Moscow State Technical University, Moscow 111005, Russia

E-mail: igorandg@gmail.com and gefedorov@mail.ru

Received 22 November 2017, revised 5 March 2018
Accepted for publication 19 March 2018
Published 16 April 2018

**Abstract**

We report on the sub-terahertz (THz) (129–450 GHz) photoresponse of devices based on single layer graphene and graphene nanoribbons with asymmetric source and drain (vanadium and gold) contacts. Vanadium forms a barrier at the graphene interface, while gold forms an Ohmic contact. We find that at low temperatures (77 K) the detector responsivity rises with the increasing frequency of the incident sub-THz radiation. We interpret this result as a manifestation of a plasmonic effect in the devices with the relatively long plasmonic wavelengths. Graphene nanoribbon devices display a similar pattern, albeit with a lower responsivity.

Supplementary material for this article is available online

Keywords: terahertz radiation, terahertz detector, graphene, graphene nanoribbon, plasma waves

(Some figures may appear in colour only in the online journal)

## 1. Introduction

The detection of radiation in the THz region of the spectrum is an important challenge, which might benefit from the availability of new nanomaterials, such as graphene [1–14]. We focus on the direct detection, in which the impinging radiation leads to an observable change of the current-voltage characteristic. The response in the sub-THz range changes with the radiation frequency, which turns out to increase with frequency (at 77 K) in contrast to most microelectronic detection techniques. We will interpret this increase as a signature of a plasmonic excitation generated by the incoming radiation.

As proposed in the early 1990s, a fast response time of field-effect transistors (FETs) involves the excitation of

[12] Author to whom any correspondence should be addressed.

 

plasma waves in a two-dimensional electron gas, with a much faster propagation time than the conventional drift time of the electron gas [15, 16]. The excitation of the plasma oscillations leads to the appearance of the rectified components of the electric field and electron density in the FET channel, associated with the nonlinearity of the electron transport (hydrodynamic nonlinearity [15, 16]). Different detectors based on III-V high mobility transistors or Si-based devices using the plasmonic effects leading to the THz signals rectification have been realized [17–24]. The strength of the plasmonic resonances depends on the plasma oscillations decay rate. The latter is determined by the scattering of the electrons (or holes) on phonons and impurities, the viscosity of the electron system and radiative damping, etc. [15, 16]. In the majority of the heterostructures in question, the plasma oscillation damping (say, the electron collision frequency) is of the same order as characteristic plasma frequencies. In such situations, the plasma oscillations are overdamped, so that the resonant response is not particularly pronounced. However, even the overdamped plasma resonances can lead to elevated values of responsivity of the plasmonic detectors, which are also interesting from the practical point of view.

The combination of the high carrier mobility and relatively low collision rates, leads to weaker plasma oscillation decay and fairly pronounced plasmonic effects in a single layer graphene (SLG) [25–29]. The first graphene FET detectors using this hydrodynamic nonlinearity, leading to the THz signals rectification, demonstrate broadband THz detection via the overdamped plasma oscillations [3, 11, 13, 30].

Here, we focus on the investigation of the frequency dependence of the detector efficiency, which is the most direct approach for the investigation of the plasmonic contribution to the response. We use the detectors of sub-THz radiation with asymmetric source and drain (vanadium and gold) contacts to SLG and graphene nanoribbons (GNR). Vanadium forms a barrier at the graphene interface and gold forms an Ohmic contact [6, 31, 32]. We demonstrate that even in the case of an SLG detector with rather modest electron mobilities, the plasma waves excitations lead to an increase of device responsivity with the increasing frequency of the incident radiation (129–450 GHz at T = 77 K). We also show that the unusual properties of the barrier at the graphene–vanadium interface explain the temperature evolution of the response, as well as the suppression of the response in the graphene nanoribbons devices.

## 2. Experimental results

### 2.1. Description of devices

Graphene, acting as the conducting channel of an FET, was put on top of an oxidized silicon wafer (see supplementary information, available online at stacks.iop.org/NANO/29/245204/mmedia). This silicon substrate was a 480 $\mu$m thick silicon wafer covered with a 500 nm thick, thermally grown $SiO_2$ layer. The doped silicon (with the room temperature resistivity of 10 $\Omega \cdot$ cm) forms a gate electrode, transparent for the sub-THz and THz radiation.

The SLG was synthesized in a home-made, cold-wall chemical vapor deposition (CVD) reactor by CVD on a copper foil with a thickness of 25 $\mu$m [33]. After the transferring of graphene onto a silicon wafer, the geometry of the device is further defined by e-beam lithography using a PMMA mask and oxygen plasma etching. Two different types of devices were made. The first type of devices were shaped as Hall bars and were used to determine transport constants of the synthesized graphene (see the supplementary information for details). The second type of devices were used for the detection of THz radiation. They were fabricated as follows: the electrical contacts to the two sides of the graphene were made with different metals having different work functions, in order to introduce electrical potential asymmetry between the two electrical contact boundaries (figures 1(a), (c)) [6, 31]. At one end of graphene (left in figure 1(a)) the contact is made of gold (Au) (with a work function of 5.1 eV) and at the other end (right in figure 1(a)) the contact material is vanadium (with a work function of 3.9 eV). In short, we will refer to these contact electrodes as gold and vanadium source and drain contacts. Since graphene is p-doped by adsorbed oxygen, vanadium forms a potential barrier at the graphene interface, whereas gold forms an Ohmic contact as shown in figure 1(a). The carrier concentration and mobility are determined from a Hall bar structure.

The source and drain contacts are connected to a spiral antenna (see figure 1(b)) to ensure a sufficiently broad band device response. We have chosen the log-spiral antenna defined in polar coordinates as $R = R_0 e^{\varphi/\beta}$ with the following parameters: the inner radius of the spiral $R_0$ equals 5.5 $\mu$m, outer radius $R_{\max} = 68$ $\mu$m and the parameter determining the rate of spiral $\beta = 3.2$. Further details of the antenna parameters and its characteristics are presented in [34]. Importantly, such an antenna is relatively easy to fabricate.

### 2.2. Device characterization and experimental set-up

A chip, with dimensions of $4 \times 4$ mm$^2$, with a device fabricated on top of it is further fixed on the flat surface of a silicon lens, in such a way that the sensing element of the device, the antenna with graphene in the center, is located in the lens focus. A special lens holder is placed inside an optical cryostat, equipped with a high-density polyethylene window. A Zytex-106 cold infrared filter is mounted in the radiation shield of the cryostat to block the 300 K background radiation. The power incident on the cryostat window is measured with a Golay cell. BWO 1 was used as a source of sub-THz radiation with the frequency of $f = 129$ GHz. It has a maximum power of radiation at the cryostat window of 1 mW, as measured by a thermistor, and the power is adjusted by a wire-grid attenuator. The sum of the losses in the silicon lens and the cryostat optical window do not exceed 5–6 dB. BWO 2 was used in the frequency range $f = 265$–450 GHz. The power at each frequency had a maximum value of about 0.6 mW.

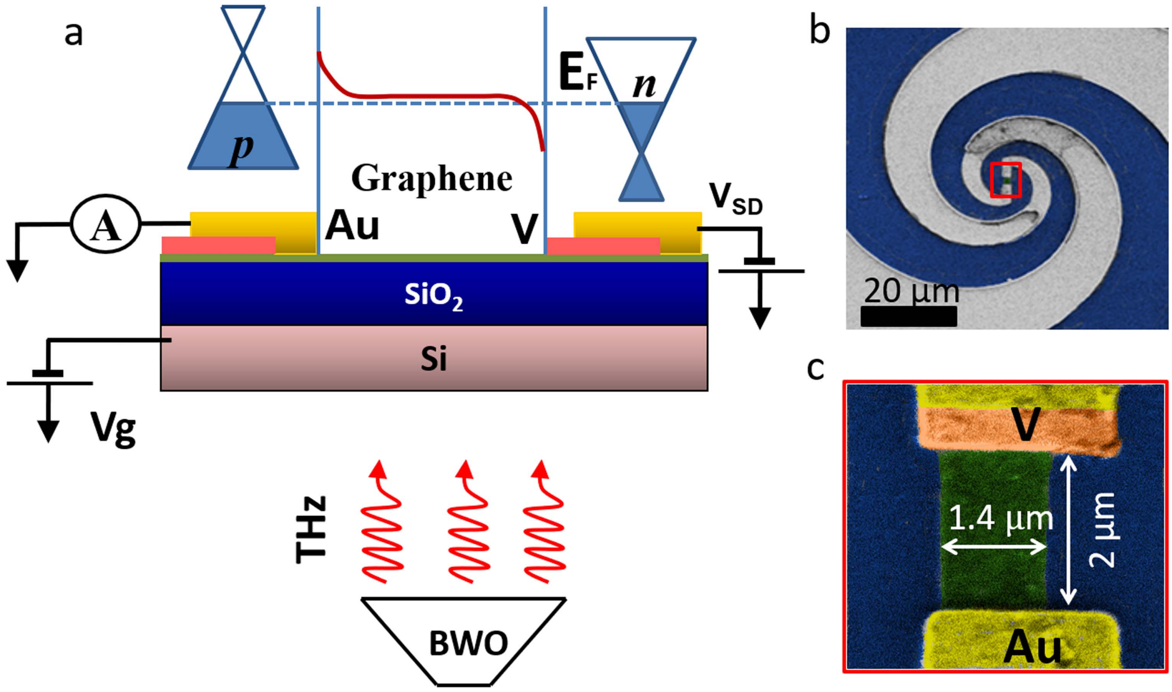


**Figure 1.** (a) Schematic representation of the transistor device, illustrating the current path between the gold and vanadium electrodes. (b) A scanning electron microscopy image of the device coupled to the radiation with a logarithmic spiral antenna made of gold (Au). The red rectangle marks the transistor channel area. (c) A typical scanning electron microscopy image of the transistor channel formed by graphene.

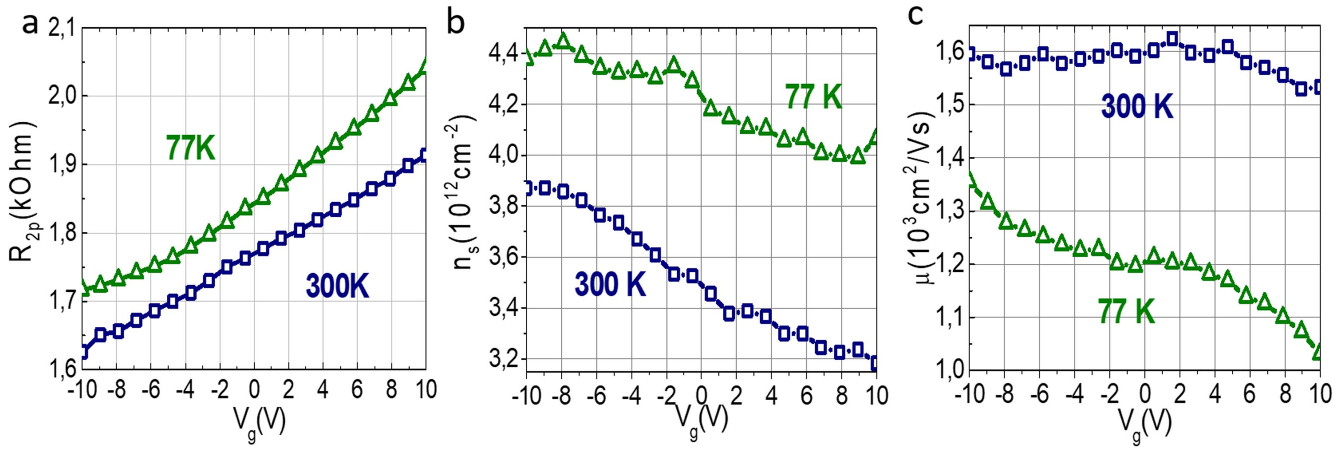


**Figure 2.** Two-probe resistance of the graphene detector device as a function of gate voltage (a). Carrier concentration (b) and hole mobility (c) extracted from the Hall voltage measurements as a function of gate voltage.

Prior to the photoresponse measurements, we measured the DC transport characteristics of the devices. Figure 2(a) shows the resistance $R_{2p}$ of the graphene devices as a function of gate voltage, measured at 300 K and 77 K. The resistance of the device increases when the gate voltage is swept from $-10$ to 10 V, indicating p-doping of graphene. Another common feature is a few percent increase of the resistance, when the temperature goes down from 300 to 77 K, which is not typical for metals. We note that a two-probe resistance $R_{2p}$ includes a temperature-dependent contact resistance.

Our four-probe transport measurements indicate that the sheet resistance of graphene is almost the same at temperatures of 300 K and 77 K, decreasing by less than 3%, while the two-probe resistance changes by more than 5%. Therefore, we associate the increase of $R_{2p}$ with the increase of contact resistance at the graphene–vanadium interface due to a barrier at this interface. We used our Hall bar devices (see SI, figure 1(b)) to determine the concentration and mobility of the CVD graphene used in our experiments, as shown in figure 2. Measuring both Hall and four-probe resistance using a PPMS-9 cryomagnetic system, we find that the carrier concentration is around $4 \cdot 10^{12}\ /\mathrm{cm}^2$. At the same time, the carriers' mobility slightly decreases upon temperature decrease from 300 to 77 K, while the scattering rate defined as $\tau^{-1} = v_F/l_{SC}$ is around 20 THz at both room temperature and 77 K. Here, $v_F \sim 10^6\ \mathrm{m\ s^{-1}}$ is the Fermi velocity and the elastic mean free path $l_{SC}$ that is found to be around 50 nm in our devices (see SI for details). These data mean that the

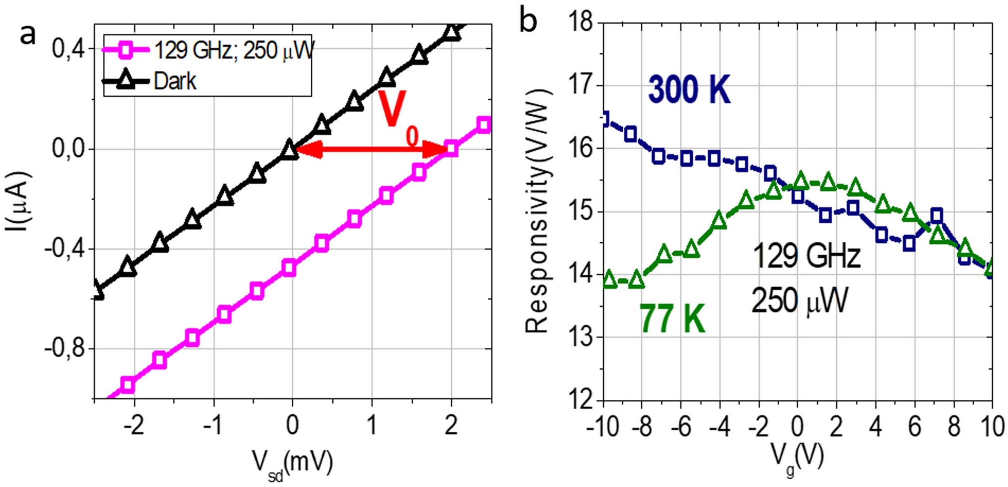


**Figure 3.** (a) I–V curves of the graphene devices measured with and without THz radiation at 300 K. (b) Responsivity of the graphene devices as a function of gate voltage measured at 300 K and 77 K.

graphene conduction is limited by defect scattering at room temperature already, with the electron–phonon scattering rate being much lower than that for defects. This is not surprising for CVD grown graphene. A decrease of conductance upon temperature lowering should be ascribed to weak localization, as further confirmed by our magnetotransport experiments, which yield a dephasing time of about 4ps at 77 K [35].

### *2.3. Photoresponse measurements*

The response of the graphene-FET to radiation is studied in the frequency range from 129 GHz–450 GHz.

First, we characterize the room temperature response of our devices to sub-THz radiation at the frequency of 129 GHz. Figure 3(a) shows the current–voltage characteristics, measured with the gate grounded, with and without the impinging radiation. When the device is exposed to 129 GHz radiation, with a power of $P = 250\,\mu$W, the I–V curve shifts to the right. As shown, the zero-current crossing was shifted by a voltage $V_0$ of about 2 mV. This DC voltage $V_0$ induced by the radiation is the response voltage $V_{RESP}$. No significant change in the differential conductance, due to the radiation, is observed at this temperature, indicating low bolometric effect contribution to the device response.

Next, we measure the gate dependence of the response voltage $V_{RESP}(V_G)$, both at room temperature and at 77 K. The results are displayed in figure 3(b), with the responsivity defined as $V_{RESP}/P$, where P is a power incident on the device with allowance for absorption in silicon (see supplementary information). As seen from the data, the responsivity at 300 K is practically independent of the gate voltage: the response decreases only slightly and monotonically with the increasing gate voltage. Similar results were obtained at the frequencies of 280 GHz, 330 GHz, 380 GHz and 445 GHz (using BWO 2). These data also show that the response is only weakly dependent on the gate voltage at room temperature. Given this lack of response dependence on gate voltage, we compare the responsivity of the devices for five frequency values in the range of 129–450 GHz, with the gate grounded.

The results are shown in figure 4(a). As seen from figure 4(a), at room temperature the responsivity decreases as the frequency is increased from 14 V W$^{-1}$ at 129 GHz to 3 V W$^{-1}$ at 440 GHz. Similar measurements for the same fixed frequencies were carried out at 77 K. The results are shown in figure 4(b). At 77 K the responsivity also weakly depends on the gate voltage (figure 3(b)). However, the frequency dependence of the responsivity at 77 K is strikingly different from that at 300 K. At 77 K, the responsivity increases as the frequency increases within the range of 129 GHz–450 GHz.

## 3. Discussion

In previous discussions on the response of asymmetric graphene or carbon nanotube devices to THz radiation, the focus was made on the rectification of alternating current (AC) due to the photothermal or diode effects [6, 8], which in some cases were combined [36, 37]. In the case of a pure photo-thermoelectric effect, non-linearity is the result of either non-uniform doping of the channel or non-uniform heating of the channel as it is exposed to radiation. In both cases, a DC voltage signal should be proportional to the increase of the electron temperature. Alternatively, within the diode response scenario, the non-linearity occurs due to presence of a barrier at either electrode.

The most important feature observed in our experiments is the qualitative change of the frequency dependence of the device responsivity upon a decrease of the temperature from 300 K to 77 K. (figure 4). As the temperature is lowered, the character of the dependence of the responsivity on frequency changes from a decreasing to an increasing one. First of all, we checked that this effect could not be ascribed to a strong temperature effect on the impedance matching of the antenna with the load (the graphene device), whose complex conductivity as a function of frequency may strongly change with temperature [13, 38, 39]. We have ruled out this possibility, performing electrodynamic simulations accounting for the

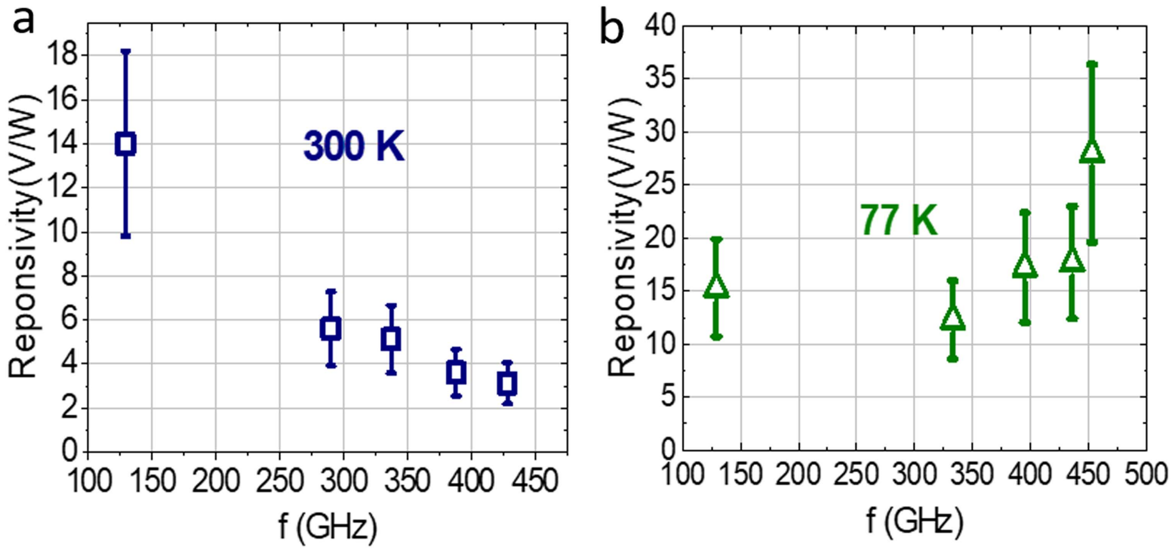


**Figure 4.** Responsivity of the graphene devices as a function of the radiation frequency measured at 300 K (a) and 77 K (b).

antenna geometry. Radiation transmittance through the silicon substrate and device intrinsic impedance neglect not accounting for the plasma wave excitation (see SI).

For further analysis it is essential to note that the excitation of plasmons may change the value of the response voltage, whether it occurs due to the nonlinearity or due to the photothermal effect [40, 41].

The role of plasma wave excitation in the channel was considered by Ryzhii and Shur in 2006 [40]. It was shown that for a plasmonic response, the device responsivity at a given frequency is determined by the ratio of the fundamental plasmon resonance frequency $\Omega$ to the scattering rate $\tau^{-1}$. Since our DC transport measurements clearly show that the scattering rate does not depend on temperature, the model developed in [40] cannot be applied directly to our case. In the case of the photothermoelectric scenario, suggested by Cai *et al* [6], the model considered in [40] should be applicable. However, this model cannot explain the observed frequency dependence. On the other hand, the non-linearity that occurs due to the presence of a Schottky barrier also involves a shunting capacitor, which affects the frequency dependence of the response. Therefore, we consider more closely the effect of rectification due to presence of a barrier at one electrode. It is known, for example [42–45], that for p-type graphene, at the contact with the metal that has a low work function, there is an n-part, creating a p–n junction in graphene, which dominates the contact resistance. In our case, it could also be a thin oxide layer at the interface between graphene and the vanadium metal. We note that at a non-zero frequency, the barrier is 'shunted' by its capacitance, so the amplitude of the current through the barrier is less than that through the channel.

First, we have modified the model considered in the [40] in order to account for the capacitance of the barrier and the excitation of plasma waves in the 2D graphene channel. We arrive at the following formulas for the gated detector voltage (in V/W) responsivity as a function of incident radiation frequency $\omega$:

$$\beta_\omega = \frac{\beta_0}{\left| \cos\left[\frac{\pi\sqrt{\omega(\omega+i\gamma)}}{2\Omega}\right] + a_\omega \sin\left[\frac{\pi\sqrt{\omega(\omega+i\gamma)}}{2\Omega}\right] \right|^2}. \quad (1)$$

In equation (1), the frequency:

$$\Omega = \frac{\pi^{5/4} v_W}{L}\sqrt{\left(\frac{e^2}{\kappa_g v_W \hbar}\right) W_g \sqrt{n}}\,, \quad (2)$$

is the characteristic plasma frequency for the gated channel [26], $n$ is the electron density in the quasi-neutral section of the channel with the length close to the net channel length $L$, $W_g$ is the gate layer thickness, $v_W \simeq 10^8$ cm s$^{-1}$ is the characteristic electron velocity in graphene, $k$ is the effective dielectric constant (depending on the dielectric constants above and beneath the graphene (or for the graphene nanoribbon), $\gamma = \tau^{-1} + \xi(2\pi/\lambda)^2$ [16] is the plasma oscillations decay rate, $\tau^{-1}$ is the frequency of electron collisions with impurities, phonons, and edges (in graphene), $\xi$ is the electron viscosity, $\lambda = 4$ L is the plasma wavelength and $\beta_0$ is low frequency responsivity. The quantity

$$a_\omega = -ib\left(\frac{2\Omega}{\pi\nu}\right)\frac{(\omega + i\tau^{-1})}{\sqrt{\omega(\omega + i\gamma)}}(1 - i\omega\tau_S) \quad (3)$$

characterizes the ratio of the AC channel and the Schottky junction conductances. Here, $\tau_S = C_S{}^* r_S$ and $C_S$ are the Schottky junction recharging time (through the Schottky junction) and capacitance, respectively, and $b = L/\sigma_0 r_S = r_{2DES}/r_S$, $r_S = (dJ_S/dV)^{-1}$ is the Schottky junction differential resistance, where $J_S(V)$ is the junction current–voltage characteristic, and $r_{2DES}$ is the DC resistance of the quasi-neutral channel section. Deriving $a_\omega$, we have assumed that the AC conductivity of the 2DES channel is equal to $\sigma_\omega = \sigma_0\, \tau^{-1}/(\tau^{-1} - i\omega)$, where $\sigma_0$ is the DC conductivity.

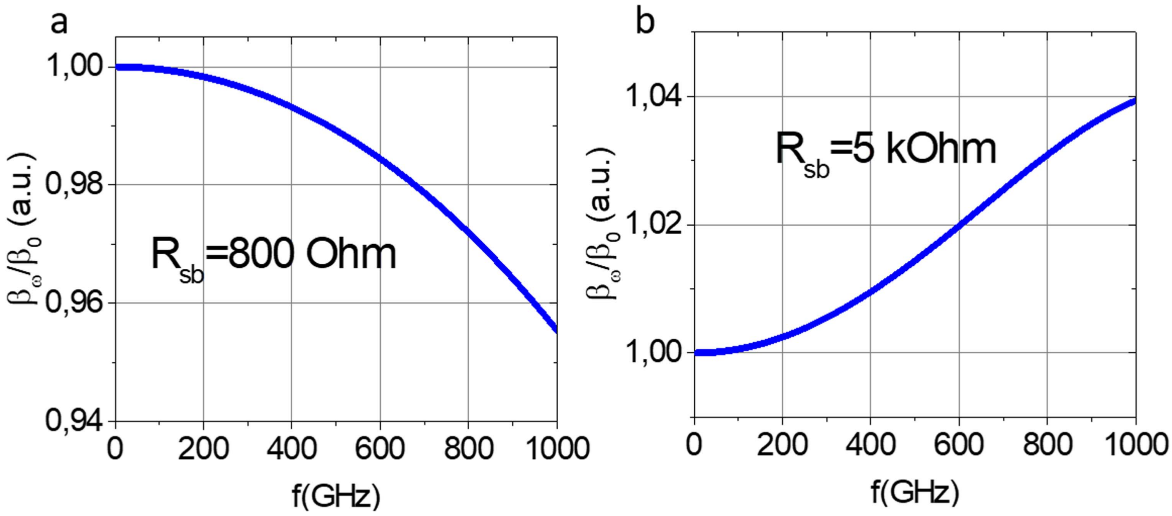


**Figure 5.** (a), (b) Calculated frequency dependence of the rectified current normalized at its value at zero frequency (equation (1)). The parameters input into the calculations are $\Omega = 30 * 10^{12}\,s^{-1}$, $\tau^{-1} = 18 * 10^{12}\,s^{-1}$, $C_s = 4 * 10^{-17}$F; $r_{2d} = 2$ kOhm.

Based on the temperature evolution of the DC transport, we argue that the only temperature-dependent parameter in the above equations is the Schottky junction recharging time, which is proportional to the barrier resistance. Figures 5(a) and (b), show the frequency evolution of the parameter $\beta_\omega/\beta_0$ for two values of $\tau_S$. We see that the responsivity is a rising function of frequency for large enough values of $\tau_S$ and decreasing otherwise. Other parameters input into the calculations are provided in the figure caption.

We therefore conclude that the observed temperature evolution of the responsivity can be explained by a significant increase in the barrier DC resistance, as the temperature is lowered. This, in turn, points to the thermally activated transport or the thermally assisted tunneling through the barrier. A simple model of transport through the barrier, accounting for the thermal activation, only predicts a zero frequency limit of device responsivity to be inversely proportional to temperature, which is not the case in our experiments. We also do not observe any significant increase of the two-probe resistance of our devices.

Thus, the observed temperature evolution of the responsivity can be explained by a significant increase in the barrier resistance, while the DC transport data contradict this statement. The only way, in our view, to resolve this contradiction is to associate the barrier not with an oxide layer at the interface between graphene and the metal (vanadium), but with a barrier existing for charge carriers that cross the p–n junction non-normally. The transport of carriers through a p–n junction in graphene depends on the angle between the normal to the interface and electron direction. For normally incident electrons, there is no energy barrier and they shunt the nonlinear transport. At the same time, the current of non-normally incident electrons is a non-linear function of the applied voltage [45, 46].

In order to verify the possible scenario of rectification due to a p–n junction at the V electrode, we fabricated the samples of graphene nanoribbons (figure 6(a) inset). In the case of the nanoribbons, a smaller channel width should lead to a more collimated motion of the charge carriers, so that the fraction of normally incident carriers is larger, causing a smaller response value (figure 6(b)).

The obtained results are in good agreement with this prediction. The room temperature measurements of the nanoribbon devices show that the transport characteristics for nanoribbon and graphene devices are similar. Figure 6(a) shows the sheet conductance $G_{sq}$ of typical GNR and SLG devices as a function of the gate voltage measured at 300 K. The resistance per square is almost the same for GNR and SLG devices indicating a small contribution of the contact resistance in all cases.

At 300 K, the photoresponse measurements indicate that the responsivity decreases with the radiation frequency (responsivity at frequency 129 GHz is 1 V W$^{-1}$) and the response to the radiation becomes too small to be detectable at the frequency above 280 GHz. Figure 6(c) shows the frequency dependence of the nanoribbon device responsivity at 77 K. As seen from this figure, the responsivity of the nanoribbon devices is much smaller than that of the graphene devices, but it also increases in the frequency range of 129–450 GHz.

To conclude, we have shown that plasma waves can affect the frequency dependence of the response of a graphene lateral Schottky diode, even in the graphene devices with rather modest electron mobilities far from the first plasmon resonance, which should be observed at 4.9 THz for our channel geometry and carrier concentration. A strong enhancement of the response is observed at moderately low temperatures, when the frequency is increased towards the plasma resonance frequency. In order to reach the full resonance in the studied frequency range, we should use a better quality graphene (such as h-BN-encapsulated graphene with a high mobility) and a longer channel.

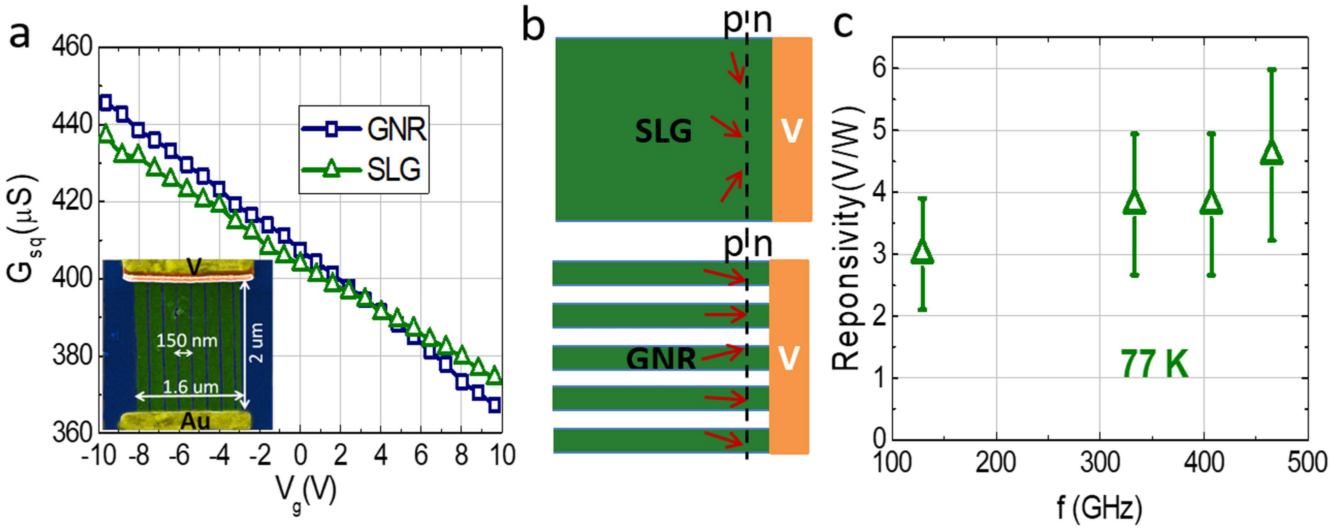


**Figure 6.** (a) Sheet conductance per square of the GNR and SLG devices as a function of gate voltage at 300 K, inset: electron image of the transistor channel formed by GNR. The length of the SLG device channel is 1 μm, the width is 1.4 μm (total area: 1.4 $\mu m^2$). The length of the GNR device channel is 2 μm, total channel width is 1.6 μm; total GNR width −1.1 $\mu$m (total area: 2.2 $\mu m^2$). (b) Schematic representation of carriers transport through a p–n junction near vanadium electrode. (c) Responsivity of GNR devices as a function of the radiation frequency measured at 77 K.

## Acknowledgments

This work was partly supported by the Russian Science Foundation, Grant No. 17-72-30036 (section 2 experimental results) and Russian Foundation for Basic Research (RFBR) (15-02-07787). GG acknowledges the financial support from the Ministry of Education and Science of the Russian Federation, State Task No. 3.7328.2017/LS. The work at RIEC was supported by the Japan Society for Promotion of Science, KAKENHI Grant No. 16H06361. The work performed into the section 3 discussion was supported by the Russian Science Foundation, Grant No. 14-29-00277. EO thanks the RFBR for support, research project No. 16-02-00979. MR thanks the RFBR for support, research project No. 16-32-60203 mol_a_dk. SS acknowledges the financial support from the RFBR under Grant No. 16-32-00622. VL thanks the RFBR for support, research project No. 18-07-01379. The work at IUHFSE was supported by the grant of the RFBR No. 16-29-03033. VR is grateful to V Mitin, V E Karasik, and P P Maltzev for fruitful discussions and support. IG is grateful to Professor T M Klapwijk for helpful discussions. Magneto-transport measurements have been done using research equipment of the P N Lebedev Physical Institute Shared Facility Center. The work at RPI was supported by the US Army Research Office. SEM was performed using the equipment of the MIPT Shared Facilities Center and with financial support from the Ministry of Education and Science of the Russian Federation (Grant No. RFMEFI59417X0014).

## ORCID iDs

I A Gayduchenko https://orcid.org/0000-0003-2560-6503
E D Obraztsova https://orcid.org/0000-0003-3001-2996

## References

[1] Ryzhii V, Ryzhii M, Shur M S, Mitin V, Satou A and Otsuji T 2016 Resonant plasmonic terahertz detection in graphene split-gate field-effect transistors with lateral p–n junctions *J. Phys. D: Appl. Phys.* **49** 315103315103
[2] Ryzhii V, Satou A, Otsuji T, Ryzhii M, Mitin V and Shur M S 2013 Dynamic effects in double graphene-layer structures with inter-layer resonant-tunneling negative conductivity *J. Phys. D: Appl. Phys.* **46** 315107
[3] Vicarelli L, Vitiello M S, Coquillat D, Lombardo A, Ferrari A C, Knap W, Polini M, Pellegrini V and Tredicucci A 2012 Graphene field-effect transistors as room-temperature detectors *Nat. Mater.* **11** 865
[4] Spirito D, Coquillat D, De Bonis S L, Lombardo A, Bruna M, Ferrari A C, Pellegrini V, Tredicucci A, Knap W and Vitiello M S 2014 High performance bilayer-graphene terahertz detectors *Appl. Phys. Lett.* **104** 061111
[5] Bianco F, Perenzoni D, Convertino D, De Bonis S L, Spirito D, Perenzoni M, Coletti C, Vitiello M S and Tredicucci A 2016 Terahertz detection by epitaxial-graphene field-effect-transistors on silicon carbide *Appl. Phys. Lett.* **107** 131104
[6] Cai X *et al* 2014 Sensitive room-temperature terahertz detection via the photothermoelectric effect in graphene *Nat. Nanotechnol.* **9** 814–9
[7] Ryzhii V, Otsuji T, Ryzhii M, Mitin V and Shur M S 2015 Resonant plasmonic terahertz detection in vertical graphene-base hot-electron transistors *J. Appl. Phys.* **118** 204501
[8] Jiayue T, Muthee M, Chen S-Y, Yngvesson S K and Yan J 2015 Antenna enhanced graphene THz emitter and detector *Nano Lett.* **15** 5295–301
[9] Qin H *et al* 2017 Room-temperature, low-impedance and high-sensitivity terahertz direct detector based on bilayer graphene field-effect transistor *Carbon* **116** 760–5
[10] Mittendorff M, Winner S, Kamann J, Eroms J, Weiss D, Schneider H and Helm M 2013 Ultrafast graphene-based broadband THz detector *Appl. Phys. Lett.* **103** 021113
[11] Muraviev A V, Rumyantsev S L, Liu G, Balandin A A, Knap W and Shur M S 2013 Plasmonic and bolometric

terahertz detection by graphene field-effect transistor *Appl. Phys. Lett.* **103** 181114
[12] Cai X, Sushkov A B, Jadidi M M, Nyakiti L O, Myers-Ward R L, Gaskill D K, Murphy Th E, Fuhrer M S and Dennis D H 2015 Plasmon-enhanced terahertz photodetection in graphene *Nano Lett.* **15** 4295–302
[13] Zak A, Andersson M A, Bauer M, Matukas J, Lisauskas A, Roskos H G and Stake J 2014 Antenna-integrated 0.6 THz FET direct detectors based on CVD graphene *Nano Lett.* **14** 5834–8
[14] Degl'Innocenti R *et al* 2016 Fast room-temperature detection of terahertz quantum cascade lasers with graphene-loaded bow-tie plasmonic antenna arrays *ACS Photonics* **3** 1747–53
[15] Dyakonov M I and Shur M S 1996 Plasma wave electronics: novel terahertz devices using two-dimensional electron fluid *IEEE Trans. Electron Dev.* **43** 1640
[16] Dyakonov M and Shur M 1993 Shallow water analogy for a ballistic field effect transistor: New mechanism of plasma wave generation by dc current *Phys. Rev. Lett.* **71** 2465
[17] Popov V V, Koudymov A N, Shur M and Polischuk O V 2008 Tuning of ungated plasmons by a gate in the field-effect transistor with two-dimensional electron channel *J. Appl. Phys.* **104** 024508
[18] Giliberti V, Di Gaspare A, Giovine E, Ortolani M, Sorba L, Biasiol G, Popov V V, Fateev D V and Evangelisti F 2016 Downconversion of terahertz radiation due to intrinsic hydrodynamic nonlinearity of a two-dimensional electron plasma *Phys. Rev.* B **91** 165313
[19] Muravev V M and Kukushkin I V 2012 Plasmonic detector/spectrometer of subterahertz radiation based on two-dimensional electron system with embedded defect *Appl. Phys. Lett.* **100** 082102
[20] Di Gaspare A, Casini R, Foglietti V, Giliberti V, Giovine E and Ortolani M 2012 Terahertz current oscillations in a gated two-dimensional electron gas with antenna integrated at the channel ends *Appl. Phys. Lett.* **100** 203504
[21] Dyer G C, Preu S, Aizin G R, Mikalopas J, Grine A D and Reno J L 2012 Enhanced performance of resonant sub-terahertz detection in a plasmonic cavity *Appl. Phys. Lett.* **100** 083506
[22] Knap W, Teppe F, Meziani Y, Dyakonova N, Lusakowski J, Boeuf F, Skotnicki T, Maude D, Rumyantsev S and Shur M S 2004 Plasma wave detection of sub-terahertz and terahertz radiation by silicon field eeffectt transistors *Appl. Phys. Lett.* **85** 675–7
[23] Knap W, Deng Y, Rumyantsev S, Lu J-Q, Shur M S, Saylor C A and Brunel L C 2002 Resonant detection of subterahertz radiation by plasma waves in a submicron field-effect transistor *Appl. Phys. Lett.* **80** 3433
[24] Otsuji T, Hanabe M and Ogawara O 2004 Terahertz plasma wave resonance of two-dimensional electrons in InGaP/InGaAs/GaAs high-electron mobility transistors *Appl. Phys. Lett.* **85** 2119
[25] Grigorenko A N, Polini M and Novoselov K 2012 Graphene plasmonics *Nat. Photon.* **6** 749–58
[26] Tomadin A and Polini M 2013 Theory of the plasma-wave photoresponse of a gated graphene sheet *Phys. Rev.* B **88** 205426
[27] Ryzhii V, Satou A and Otsuji T 2007 Plasma waves in two-dimensional electron-hole system in gated graphene heterostructures *J. Appl. Phys.* **101** 024509
[28] Svintsov D, Vyurkov V, Yurchenko S, Otsuji T and Ryzhii V 2012 Hydrodynamic model for electron-hole plasma in graphene *J. Appl. Phys.* **111** 083715
[29] Svintsov D, Vyurkov V, Ryzhii V and Otsuji T 2013 Hydrodynamic electron transport and nonlinear waves in graphene *Phys. Rev.* B **88** 245444
[30] Shur M, Muraviev A V, Rumyantsev S L, Knap W, Liu G and Balandin A A 2013 Plasmonic and bolometric terahertz graphene sensors *Proc. of 2013 IEEE Sensors Conf.*
[31] Mueller T, Xia F and Avouris P 2010 Graphene photodetectors for high-speed optical communications *Nat. Photon.* **4** 297–301
[32] Zhong H, Zhang Z, Chen B, Xu H, Yu D, Huang L and Peng L-M 2015 Realization of low contact resistance close to theoretical limit in graphene transistors *Nano Res.* **8** 1669 -179
[33] Rybin M, Pereyaslavtsev A, Vasilieva T, Myasnikov V, Sokolov I, Pavlova A, Obraztsova E A, Khomich A, Ralchenko V and Obraztsova E D 2016 Efficient nitrogen doping of graphene by plasma treatment *Carbon* **96** 196–202
[34] Shurakov A, Seliverstov S, Kaurova N, Finkel M, Voronov B and Goltsman G 2012 Input bandwidth of hot electron bolometer with spiral antenna *IEEE Transactions on Terahertz Science and Technology* **2** 400–5
[35] Tikhonenko F V, Horsell D W, Gorbachev R V and Savchenko A K 2008 Weak localization in graphene flakes *Phys. Rev. Lett.* **100** 056802
[36] Gayduchenko I, Kardakova A, Fedorov G, Voronov B, Finkel M, Jimenez D, Morozov S, Presniakov M and Goltsman G 2015 Response of asymmetric carbon nanotube network devices to sub-terahertz and terahertz radiation *J. Appl. Phys.* **118** 194303
[37] Fedorov G, Gayduchenko I, Titova N, Gazaliev A, Moskotin M, Kaurova N, Voronov B and Goltsman G 2018 Carbon nanotube based schottky diodes as uncooled terahertz radiation detectors *Phys. Status Solidi* B **255** 1700227
[38] Giliberti V *et al* 2017 Loading the antenna gap with two-dimensional electron gas transistors: a versatile approach for the rectification of free-space radiation *ACS Photon.* **4** 837–45
[39] Yao Y, Kats M A, Genevet P, Yu N, Song Y, Kong J and Capasso F 2013 Broad electrical tuning of graphene-loaded plasmonic antennas *Nano Lett.* **13** 1257–64
[40] Ryzhii V and Shur M S 2006 Resonant terahertz detector utilizing plasma oscillations in two-dimensional electron system with lateral Schottky junction *Jpn. J. Appl. Phys.* **45** L1118
[41] Ryzhii V *et al* 2016 Two-dimensional plasmons in lateral carbon nanotube network structures and their effect on the terahertz radiation detection *J. Appl. Phys.* **120** 044501
[42] Young A F and Kim P 2009 Quantum interference and Klein tunnelling in graphene heterojunctions *Nat. Phys.* **5** 222–6
[43] Maher P *et al* 2014 Tunable fractional quantum Hall phases in bilayer graphene *Science* **345** 61–4
[44] Calado V E *et al* 2015 Ballistic josephson junctions in edge-contacted graphene *Nat. Nanotechnol.* **10** 761–4
[45] Katsnelson M I, Novoselov K S and Geim A K 2006 Chiral tunnelling and the Klein paradox in graphene *Nat. Phys.* **2** 620–5
[46] Sutar S, Comfort E S, Liu J, Taniguchi T, Watanabe K and Lee J U 2012 Angle-dependent carrier transmission in graphene p−n junctions *Nano Lett.* **12** 4460–4